ARTICLES

Journal of Semiconductors
(2021) 42, 122701
doi: 10.1088/1674-4926/42/12/122701

>35% 5-junction space solar cells based on the direct bonding technique

Xinyi Li, Ge Li, Hongbo Lu, and Wei Zhang†

Shanghai Institute of Space Power-sources, Shanghai 200245, China

Abstract: Multijunction solar cells are the highest efficiency photovoltaic devices yet demonstrated for both space and terrestrial applications. In recent years five-junction cells based on the direct semiconductor bonding technique (SBT), demonstrates space efficiencies >35% and presents application potentials. In this paper, the major challenges for fabricating SBT 5J cells and their appropriate strategies involving structure tunning, band engineering and material tailoring are stated, and 4-cm^2 35.4% (AM0, one sun) 5J SBT cells are presented. Further efforts on detailed optical managements are required to improve the current generating and matching in subcells, to achieve efficiencies 36%–37%, or above.

Key words: III–V; multijunction; solar cells; high efficiency; semiconductor bonding

Citation: X Y Li, G Li, H B Lu, and W Zhang, >35% 5-junction space solar cells based on the direct bonding technique[J]. *J. Semicond.*, 2021, 42(12), 122701. http://doi.org/10.1088/1674-4926/42/12/122701

1. Introduction

The pursuing of higher efficiencies is always one of the most important activities for photovoltaics community. III–V multijunction solar cells (MJSCs) are the highest efficiency photovoltaic devices yet demonstrated, for both space and terrestrial applications, among all promising technologies. Nowadays over 90% space missions use high efficiency MJSCs as the major power-sources. The higher efficiencies are extremely leveraging for spacecrafts, since they reduce all area-related weights of solar panels required for a given power output, which would reduce the launch cost and/or increase the payloads. Solar cells with efficiencies in excess of 36% have been specifical required for ongoing missions in China's Lunar Exploration Program (CLEP). It motivates the evolution of the MJSC architectures to achieve higher efficiency, by reducing carrier thermalization losses during energy conversion.

Recently high efficiency devices with four- to six-junction designs have been fabricated through two different pathways termed SBT solar cells and inverted metamorphic (IMM) solar cells, respectively. SBT 5J cells built at Spectrolab have reached world-record one-sun efficiency of 35.8% (~36%) under the standard space spectrum (AM0) and one-sun efficiency of 38.8% under the standard terrestrial spectrum (AM1.5)[1–3]. NREL reports state-of-art IMM 6J cells with one-sun efficiency of 39.2% under the standard AM1.5[4, 5]. However, as NREL noted, the device area for IMM 6J cell is too small (0.25 cm^2) to be recognized as an outright one-sun record for which 1 cm^2 is required.

The fabrication of SBT solar cells contains the following processes, as shown in Fig. 1. Subcells are lattice-matched epitaxial grown on suitable substrates (usually GaAs and InP), while top-cells are inverted and grown with etch layers or a sacrificial layer between the substrate and active layers for further convenience. Wafers are then direct semiconductor bonded. After the removal of the one-side growth substrate, the mixture is processed following the standard III–V solar cell device art. The advantage of this approach is that all junctions in the stack are grown lattice-matched and therefore have excellent epitaxial quality, which results in higher efficiencies. Also, the bonding process supports the scale-up to 4-inch or larger wafers, which provides the foundation for further industrial applications.

We have been working on SBT MJSCs from device physics to cell fabrication since 2006. Recently, SBT 5J solar cells with efficiencies in excess of 35% under the space AM0 spectrum are demonstrated. In this paper, some key points for SBT 5J cells are stated, and their appropriate strategies are discussed.

2. Challenges in SBT 5J solar cells

2.1. Suitable subcells for SBT 5J solar cells

2.1.1. Bandgap combination

Based on features of the AM0 spectrum and detailed-balance model, the generally proposed bandgap combination of 5J devices could achieve efficiencies greater than 36% is approximately 2.10/1.70/1.40/1.13/0.88 eV, and it is supposed to produce an open-circuit voltage (V_{oc}) about 4.8 V and a short-circuit current density (J_{sc}) around 12 mA/cm^2. Using experimental bandgap-voltage offsets (W_{ocs}), feasible V_{ocs} around 4.85–4.95 V for such combination could be estimated[6].

Assuming unity quantum efficiency (QE), the maximum photogenerated current (J_{ph}) in the region from 300 to 900 nm is about 38 mA/cm^2 for cells grown on GaAs substrates. For series-stacked T3J, a total J_{ph} of 36 mA/cm^2, three-fold of the expected J_{sc}, is at least required. It implies that the average surface reflectance of T3Js must be controlled below 5%, and also the propagation of light in junctions must be carefully managed to balance the current in each subcell.

Correspondence to: W Zhang, ageli@163.net
Received 16 APRIL 2021; Revised 30 MAY 2021.
©2021 Chinese Institute of Electronics

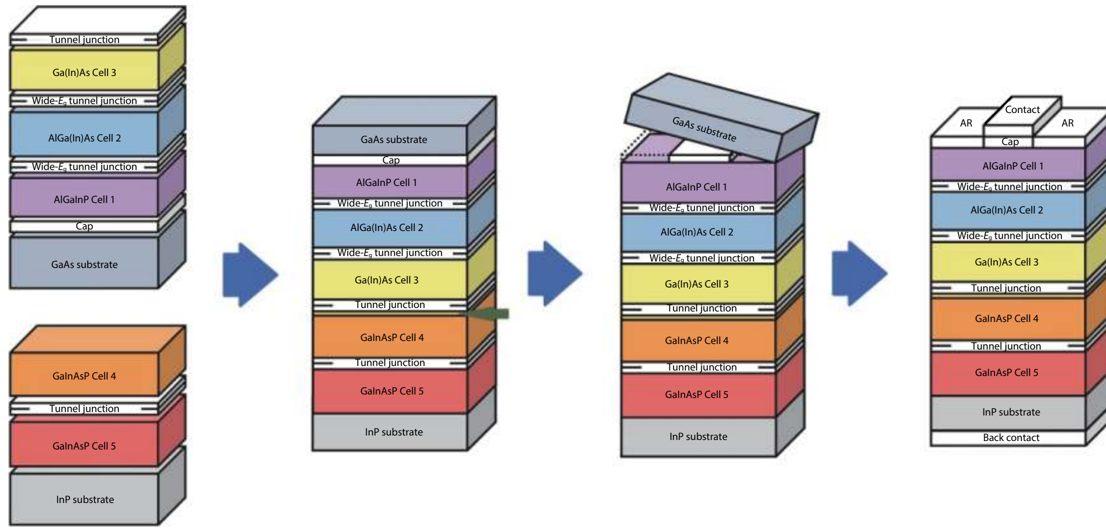

Fig. 1. (Color online) Fabrication scheme of SBT 5J cells. The arrow indicates the bonding interface.

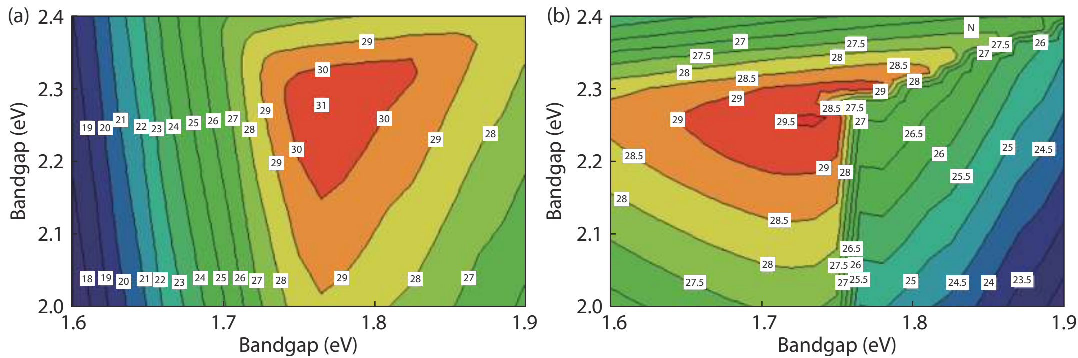

Fig. 2. (Color online) Predicted efficiencies of T3Js containing a GaAs subcell (a) without and (b) with LC. LC coefficient is set to 0.93 during calculation.

Given the fact that internal quantum efficiencies (IQEs) of individual subcells are always less than unity, it demands antireflection coatings (ARCs) with even lower reflectivity to collect as many photons as possible. Therefore, compared with V_{oc}, a J_{sc} of 12 mA/cm^2 is more challenging. The average reflectance of recent state-of-art 36% solar cells in 300–900 nm range has been minimized below 2% to deliver a J_{sc} of 12 mA/cm^2[3].

An alternative is to narrow the bandgap distance between subcells, by slightly reducing J_{sc} but increasing V_{oc} to meet efficiencies. Therefore, the bandgap combination, together with ARCs, should be coupled optimized to address requirements from both energy and optical management. As a nature of series-connected stacks, the fill factor (ff) of MJSC is pinned to a little higher value than the poorest ff of subcells. For III–V based subcells, the fill factor usually drops as the bandgap of the absorber layer decreases. Therefore, a scenario of a high-E_g top subcell current-limiting with an extra margin for J_{ph} in low-E_g bottom subcells, would be preferred for bandgap combinations to achieve higher efficiencies.

In addition, the luminescent coupling (LC) behavior complicates the tuning of bandgap combination[7–9]. Although the reabsorption of radiative recombination from top subcells adds the J_{ph} in bottom subcells, which potentially benefits the current-matching between subcells, fundamentally such process causes energy dissipation in entire carrier assemble and consequently the V_{oc}. Fig. 2 plots predicted efficiencies for T3Js as a function of bandgap combinations. It is clear that the LC behavior significantly modifies contours to lower efficiencies.

Also, parts of radiative photons could be wasted by tunnel diodes with parasitic optical absorption between subcells. Therefore, from the viewpoint of energy conversion, LC is unfavorable for high efficiency, but unavoidable. The cascade LC in multi-bandgap systems, or in MJSCs, makes it difficult to evaluate loss of output voltage and gain of J_{ph} in each subcell, since LC coefficients between subcells are extracted from the correlation of spatial coupled optical distribution and present non-linearities. It maximizes the inaccuracy of predicted efficiency from a given bandgap combination.

The preliminary results suggest that in T3Js containing GaAs subcells, the E_g of the top-cell should be at least larger than 2.1 eV, while the E_g of the mid-cell should be about 1.72 eV. A typical band diagram of such T3J is shown in Fig. 3.

2.1.2. High Al% AlGaInP top subcell

In spite of uncertainty of the bandgap combination, topcells with E_g of 2.1–2.2 eV are well-recognized as better energy harvesting of short-wavelength photons. AlGaInP, with aluminum composition around 20%, is the only option for high-E_g top subcells with material compatibility.

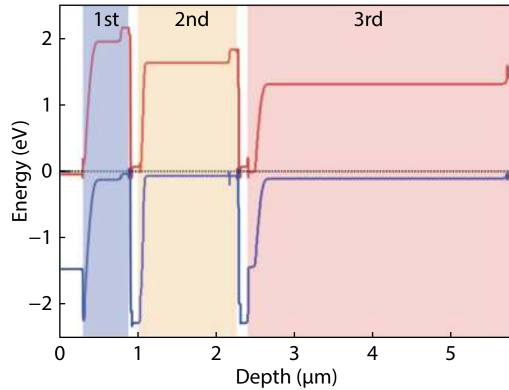

Fig. 3. (Color online) Calculated band diagram for 2.10/1.72/1.42 eV T3J.

Although AlGaInP has been widely used in microelectronics such as semiconductor lasers, LEDs and microwave power devices[10–12], the fabrication of high-E_g AlGaInP subcells are quite challenging.

As the E_g increases, the bandgap offset near the heterojunction surface shrinks, lowering the barrier height for photogenerated carriers. It leads to an increased interface recombination velocity, which is dominated by thermal emission process, and weakens the short-wavelength photon conversion efficiency.

In a traditional p–n junction, the emitter layer of the solar cell plays two distinct roles, not always complementary. On one hand, the emitter layer creates an electric field that separates the electron–hole pairs, and the minority carrier diffusion length in the layer must exceed the emitter thickness to collect as many absorbed carriers as possible. Strong deep-donor levels (DX centers) related to dopants in n-type AlGaInP limit the diffusion length, with the magnitude of the loss increasing with Al%[13].

By rising the growth temperature, it is generally considered that Al-introduced C- and/or O-related contamination would be reduced and it improves the intrinsic quality of AlGaInP layers. But indium atoms could easily evaporate from the growth surface at high temperature, and also high temperature is not favorable for the incorporation of a volatility p-type Zn dopant. Recently, it is noticed that during the growth of inverted AlGaInP solar cells, higher temperatures lead to abnormal performance deterioration.

On the other hand, the emitter is also required to spread the current laterally to grid fingers so that the current can be collected by external circuit. In this role, a high mobility in concert with a high carrier concentration leading to a low sheet resistance is preferred. For AlGaInP, the mobility is a strong function of Al composition, decreasing by a factor of two over the 0–18% composition range[14].

To address these problems, a p–n junction containing a doped low-Al% or Al-free emitter and high-Al% weak-p base, or termed reversed heterojunction, is employed to drift generated carriers with a stronger electrical field. But the bandgap offset near the heterojunction interface, together with the diffusion of the dopants can lead to unintended barriers, a valence band well and an emitter barrier, to confine and quench the carriers. It can be partially mitigated by growing a thicker undoped layer, or by grading the aluminum from low-E_g to high-E_g compositions to eliminate the various wells.

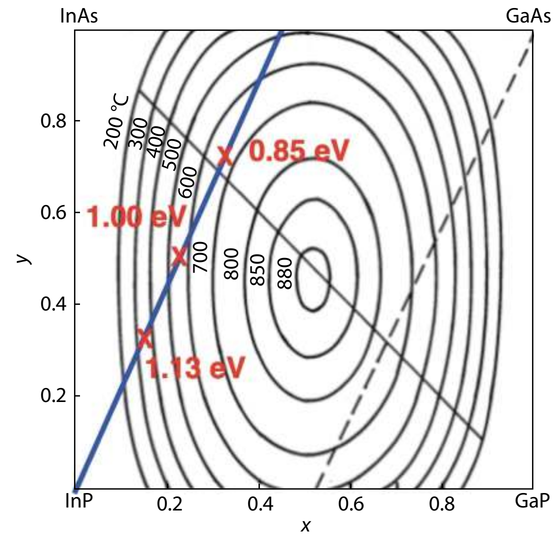

Fig. 4. Spinodal isotherms for InGaAsP quaternary. The thick solid line indicates compositions lattice-matched to InP.

2.1.3. Low-E_g quaternary bottom subcells

The general suggested bandgap combinations of bottom two junctions (B2Js) with low-E_g are around 1.13/0.88 eV. Lattice-matched InGaAsP grown on an InP substrate offers tailorable E_g from 0.74 to 1.34 eV, and presents outstanding electrical performances[15], meeting all the demands from 5J solar cells.

Growth temperature plays a critical role during the epitaxy of InGaAsP quaternary. As temperature increases, the pyrolyzation of PH_3 is greatly enhanced, and it modifies the incorporation competition between As and P atoms during growth. A slight composition deviation of V-group atoms in the quaternary results in significant variation in both E_g and the lattice-match of epilayers. Experiments reveal that some compressive strain in active layers improves the carrier lifetime in InGaAsP/InP DHs, and benefits the performances of fabricated InGaAsP-based solar cells[16].

The primary challenge linked to growth temperature is the well-known miscibility gap problem in the InGaAsP quaternary. Besides the potential material quality deterioration caused by defects and dislocations, phase separation during the growth would roughen the surface of epilayers. It leads to failures in the direct bonding process of T3J and B2J wafers.

Fig. 4 plots calculated spinodal isotherms at various temperatures for GaP–GaAs–InP–InAs system based on strictly regular solution approximation[17–19]. Compositions lattice-matched to InP with E_g of 0.85, 1.0 and 1.13 eV are marked. It shows that higher temperatures are required for the growth of stable lower-E_g InGaAsP quaternary, which makes the flow control of V-group sources quite difficult since the pyrolyzation of PH_3 is sensitive to temperature.

Metastable regions between spinodal and binodal isotherms provide choices of lower temperature for InGaAsP epitaxy. It lowers growth difficulty for low-E_g quaternary, especially for the bottommost 0.88 eV subcells, but temperature close to binodal isotherms should be avoided for the unstable potential phase.

Meanwhile, since the thickness of subcells in B2J are about 3.5–4.5 μm, the bottom subcell would undergo quite

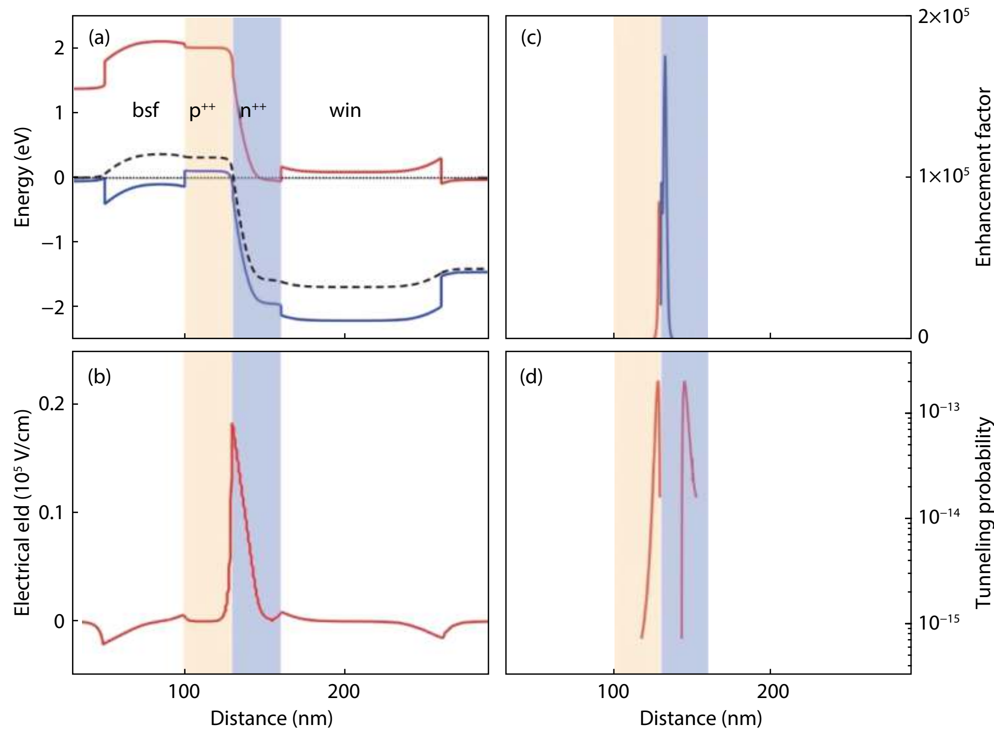

Fig. 5. (Color online) Band profile of (a) AlGaInP/AlGaAs tunnel diode, and (b) electrical field and (c, d) tunneling probability distribution in the junction.

an annealing process when the growth of top subcell is performed. Unintended dopant diffusion during such thermal history would damage abruptness of the interface, resulting in shunt junctions, and consequently poor IV curves for B2J subcells. Therefore, diffusion barriers, or designed doping profiles should be employed to mitigate dopant diffusion during growth.

2.2. Low negative differential resistance (NDR) broadband tunnel diode

To minimize current loss, tunnel diodes connecting subcells should be as transparent as possible to avoid parasitic photon absorption. For T3J, a tunnel diode with E_g above 2.0 eV is at least required to connect 2.1 and 1.7 eV subcells. Considering material compatibility, AlGaInP/AlGaAs with E_g above 2.0 eV are the most promising candidate counterparts for such tunnel diodes.

Although there is little information on its band offsets, a type-II band line-up is predicted for the above-mentioned AlGaInP/AlGaAs heterojunction tunnel diode based on density functional theory (DFT) and transfer principle, as shown in Fig. 5. The tunneling behaviors in tunnel diodes are normally dominated by non-local quantum tunneling between the conduction band and valance band (BTB process). And it couples with defect-related traps-to-bands at the hetero interface (TTB process) in type-II structure. Also, experiments reveal that thermal emission and intra-band tunneling might occur in degenerate AlGaInP/AlGaAs heterojunction. Therefore, it is of great importance to regulate the tunneling probability distribution in the junction, to improve the peak tunneling current and reduce NDR.

For AlGaAs layers, the doping level could easily be above 1×10^{20} cm^{-3} by decreasing growth temperature and V/III ratio, and increasing the C dopant mole flow. But for AlGaInP layers, the Te dopant must be introduced to obtain a degenerate doping level above 1×10^{19} cm^{-3} to avoid the band barrier. It brings trades-offs between benefits of neglectable voltage drop across the tunnel diode and risks of memory effect of Te in the following growth.

2.3. Bonding interface

Generally, GaAs and InP bonding layers are implanted on the surface T3J and B2J structures, respectively, to produce a transparent connection to avoid parasitic optical absorption. Due to the minor gap in E_g between GaAs and InP, the band offset near the interface is quite small. By heavy doping, GaAs and InP bonding layers could form counterparts of a tunnel diode, resulting in a low-resistivity interface to avoid barriers for carrier transport, as shown in Fig. 6. It also increases the density of dangling bonds in layers, which enhances van der Waals force in the initial stage of bonding and benefits the reliability of the process.

Previous reports on semiconductor lasers suggest that interface perturbations induced by the bonding process have a minor influence on the light scattering at the interface[20]. But reflectance measurements show obvious differences to the fitting results in the region of 870–930 nm, meanwhile fitting results match experimental data in the region of 350–850 nm, as shown in Fig. 7. It indicates that a thin mixture that affects photon propagation exists between bonding layers, since the bonding process involves the diffusion of atoms and the formation of new bonds.

For the purpose of better optical management in pursuing higher efficiencies, the dispersion behavior of such a mixture, probably an amorphous layer, should be established. It requires tedious sample preparing, measuring and modelling.

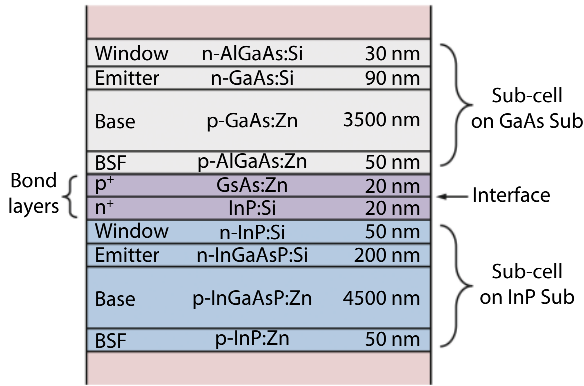

Fig. 6. (Color online) Schematic device structure after the bonding process.

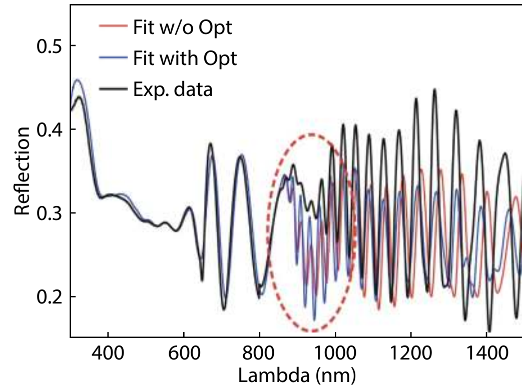

Fig. 7. (Color online) Measured surface reflection and its fitting results.

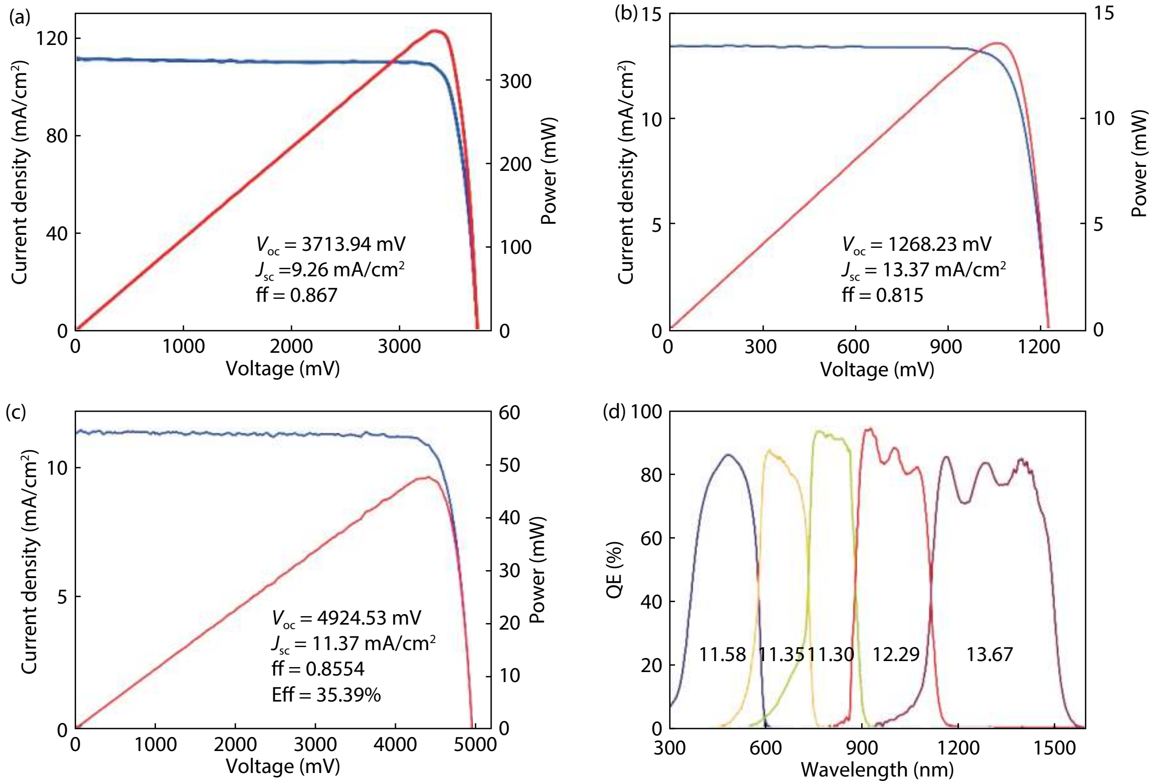

Fig. 8. (Color online) J–V curves for the representative subcells ((a)12-cm^2 T3J cell, (b) 4-cm^2 B2J cell), and (c) J–V curve and (d) corrected QE for the best representative 4-cm^2 SBT 5J cell.

3. Our recent progress in SBT 5J cells

Lattice-matched T3J with bandgap combination of 2.1/1.7/1.4 eV is inverted grown on a GaAs substrate. With band and surface engineering, potential barriers induced by surface defects and/or surface passivation are greatly reduced. A V_{oc} of 3.7 V and an ff of 0.86 are obtained under AM0 for 12-cm^2 T3J subcell, as shown in Fig. 8(a).

Lattice-matched B2J with bandgap combination of 1.13/0.88 eV is upright grown on the InP substrate. By introducing zinc diffusion barriers, the fabricated 4-cm^2 B2J subcell shows a V_{oc} above 1.2 V and an ff above 0.81 under AM0, as shown in Fig. 8(b).

SBT 5J cells are then fabricated through the direct bonding of T3J and B2J wafers. A broadband ZnS/MgF_2 ARC is deposited to minimize reflection loss. Cells are 2 × 2 cm^2 in size. Prior to I–V measurements, the spectrum simulator (X-25A, Spectrolab Inc.) is calibrated by multiple reference cells with E_g varied from 2.1 to 0.72 eV to avoid significant spectrum mismatch. All references are standardized using 35km-altitude balloon. Figs. 8(c) and 8(d) display the I–V curve and corrected QE for the best representative cell. It shows an efficiency of 35.39% under AM0 spectrum with a V_{oc} of 4.92 V, a J_{sc} of 11.37 mA/cm^2 and an ff of 0.855, while the world-record SBT 5J cell (4 cm^2) from Spectrolab presents a V_{oc} of 4.832 V, a J_{sc} of 11.77 mA/cm^2 and an ff of 0.845[3].

4. Conclusion

The major key points for fabrication of SBT 5J cells and their appropriate strategies are presented. Integrated effort on structure tunning, band engineering and material tailoring produces the devices with solar energy conversion efficiency above 35%. Compared to V_{oc}, the expected J_{sc} is much more challenging. With further improvements in optical management, a current boost of 0.5–0.7 mA/cm^2 would be achieved in SBT 5J cells, and efficiencies around 36%–37%

could be expected.

Acknowledgements

This work is supported by the National Nature Science Foundation of China (Grant No. 62004126), and Shanghai Rising-Star Program (Grant No. 19QB1403800).

References

[1] Chiu P T, Law D C, Singer S B, et al. High performance 5J and 6J direct bonded (SBT) space solar cells. 2015 IEEE 42nd Photovoltaic Specialist Conference (PVSC), 2015, 1

[2] Chiu P T, Law D C, Woo R L, et al. 35.8% space and 38.8% terrestrial 5J direct bonded cells. 2014 IEEE 40th Photovoltaic Specialist Conference (PVSC), 2014, 0011

[3] Chiu P T, Law D C, Woo R L, et al. Direct semiconductor bonded 5J cell for space and terrestrial applications. IEEE J Photovolt, 2014, 4, 493

[4] Geisz J F, France R M, Schulte K L, et al. Six-junction III–V solar cells with 47.1% conversion efficiency under 143 Suns concentration. Nat Energy, 2020, 5, 326

[5] Geisz J F, Steiner M A, Jain N, et al. Building a six-junction inverted metamorphic concentrator solar cell. IEEE J Photovolt, 2018, 8, 626

[6] King R R, Bhusari D, Boca A, et al. Band gap-voltage offset and energy production in next-generation multijunction solar cells. Prog Photovolt: Res Appl, 2011, 19, 797

[7] Tayagaki T, Reichmuth S K, Helmers H, et al. Transient analysis of luminescent coupling effects in multi-junction solar cells. J Appl Phys, 2018, 124, 183103

[8] Tayagaki T, Oshima R, Shoji Y, et al. Luminescence effects on subcell current-voltage analysis in InGaP/GaAs tandem solar cells. J Photonics Energy, 2020, 10, 025504

[9] Lim S H, Li J J, Steenbergen E H, et al. Luminescence coupling effects on multijunction solar cell external quantum efficiency measurement. Prog Photovolt: Res Appl, 2013, 21, 344

[10] Hamada H, Shono M, Honda S, et al. AlGaInP visible laser diodes grown on misoriented substrates. IEEE J Quantum Electron, 1991, 27, 1483

[11] Wu M C, Lin J F, Jou M J, et al. High reliability of AlGaInP LED's with efficient transparent contacts for spatially uniform light emission. IEEE Electron Device Lett, 1995, 16, 482

[12] Zaknoune M, Schuler O, Mollot F, et al. 0.1 μm $(Al_{0.5}Ga_{0.5})_{0.5}In_{0.5}P/In_{0.2}Ga_{0.8}As/GaAs$ PHEMT grown by gas source molecular beam epitaxy. Electron Lett, 1999, 35, 1776

[13] Heckelmann S, Lackner D, Karcher C, et al. Investigations on $Al_xGa_{1-x}As$ solar cells grown by MOVPE. IEEE J Photovoltaics, 2015, 5, 446

[14] Steiner M A, France R M, Perl E E, et al. Reverse heterojunction (Al)GaInP solar cells for improved efficiency at concentration. IEEE J Photovolt, 2020, 10, 487

[15] Lu H B, Li X Y, Zhang W, et al. MOVPE grown 1.0 eV InGaAsP solar cells with bandgap-voltage offset near to ideal radiative recombination limit. Sol Energy Mater Sol Cells, 2019, 196, 65

[16] Lu H B, Li G, Li X Y, et al. Small lattice-mismatched InGaAsP: Material characterization and application in solar cells. Chin J Lumin, 2020, 41, 351

[17] Onabe K. Calculation of miscibility gap in quaternary InGaPAs with strictly regular solution approximation. Jpn J Appl Phys, 1982, 21, 797

[18] Ono K, Takemi M. Anomalous behavior of phase separation of InGaAsP on GaAs substrates grown by MOVPE. J Cryst Growth, 2007, 298, 41

[19] LaPierre R R, Okada T, Robinson B J, et al. Spinodal-like decomposition of InGaAsP(100) InP grown by gas source molecular beam epitaxy. J Cryst Growth, 1995, 155, 1

[20] Ram R J, Dudley J J, Bowers J E, et al. GaAs to InP wafer fusion. J Appl Phys, 1995, 78, 4227

Xinyi Li received his PhD in Material Physics and Chemistry from the University of Science and Technology of China. Now he works in the Shanghai Institute of Space Power-Sources as a senior engineer. His research focuses on space energy harvesting, including next-generation high-efficiency photovoltaics, III–V epitaxy, and advanced process.

Ge Li received his BS and MS degrees in Environmental Science and Engineering from Shanghai Jiao Tong University in 2015 and 2018. He is currently working at the Shanghai Institute of Space Power-Sources. His research interests are mainly engaged in multijunction solar cells.

Hongbo Lu received his PhD in Microelectronics and Solid-State Electronics from University of Chinese Academy of Sciences. Now he works in the Shanghai Institute of Space Power-Sources as a senior engineer, mainly engaged in the development of optoelectronic devices based on group III–V material, with rich experience in solar cells and infrared detectors.

Wei Zhang received his BS degree from the School of Material Science, Wuhan University of Science and Technology in 1999, and PhD degree in Micro-electronics and Solid-State Electronics from the Institute of Semiconductors, Chinese Academy of Sciences, in 2004. Following postdoc work on single photon sources at the Hokkaido University in Japan, he joined the Shanghai Institute of Space Power-Sources in 2005. His research interests include the physics of opto-electronic devices, software development, etc.